

NumDiff Project 2

Peder Eggen Skaug, Ole Kristian Skogly, Isak Ytrøy

March 27, 2022

1 Introduction

In this project we are looking at heat distribution in anisotropic materials and a variable coefficient transport equation. Anisotropic materials shows different properties in different directions, in this report we will specifically look into anisotropic heatflow.

2 Heat distribution in anisotropic materials

2.1 The numerical scheme and it's properties

To study anisotropic heatflow we must utilize the following partial differential equation, based on Fourier's law:

$$-\nabla \cdot (\kappa \nabla T) = F, \quad (1)$$

κ is the heat conductivity matrix, and F represents potential internal heat sources in the material. We begin by discretizing the equation with second order central differences in the directions \vec{d}_1 and \vec{d}_2 .

$$\nabla(\kappa \nabla T) = a \partial_x^2 U + (\vec{d}_2 \cdot \nabla)^2 U = a \cdot \frac{U_{m+1}^n - 2U_m^n + U_{m-1}^n}{h^2} + \frac{U_{m+1}^{n+1} - 2U_m^n + U_{m-1}^{n-1}}{h^2} \quad (2)$$

We want to show that the scheme (2) is monotone. Rewriting the discretised expression such that we have the U_m^n -term on the left hand side we get:

$$(2a + 2)U_m^n = aU_{m+1}^n + aU_{m-1}^n + U_{m+1}^{n+1} + U_{m-1}^{n-1} + h^2 F \quad (3)$$

From the expression above we see that all coefficients in front of the U -terms are positive, since we have $a > 0$ by definition. Further we define the coefficient in front of U_m^n as:

$$\beta = 2a + 2$$

and the sum of the coefficients in front of the U -terms on the right hand side as:

$$\gamma = a + a + 1 + 1 = 2a + 2.$$

Since all coefficients are positive and $\beta \geq \gamma$, we have shown that the scheme is monotone. The figure below shows the stencil for the scheme.

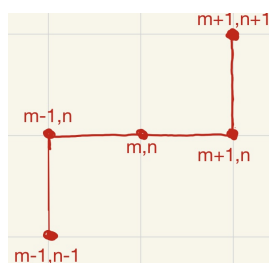


Figure 1: This is the stencil for the scheme.

To show L^∞ stability we need a comparison function, we define ϕ as:

$$\phi = \frac{1}{2}x(1-x).$$

We will use this comparison function ϕ , and the discrete maximum principle(DMP from now on) to show that the scheme is L^∞ -stable. We start with $-\mathcal{L}_h\phi$:

$$-\mathcal{L}_h\phi = \frac{(2a+2)}{h^2}\phi_m^n - \frac{a}{h^2}\phi_{m+1}^n - \frac{a}{h^2}\phi_{m-1}^n - \frac{1}{h^2}\phi_{m+1}^{n+1} - \frac{1}{h^2}\phi_{m-1}^{n-1} \quad (4)$$

Inserting the expressions for the ϕ -terms into (4), we get that $-\mathcal{L}_h\phi$ is equal to:

$$\frac{(2a+2)}{2h^2}x_m(1-x_m) - \frac{a}{2h^2}(x_m+h)(1-x_m-h) - \frac{a}{2h^2}(x_m-h)(1-x_m+h) - \frac{1}{2h^2}(x_m+h)(1-x_m-h) - \frac{1}{2h^2}(x_m-h)(1-x_m+h)$$

This expression sums up to $1 + a \geq 1$, i.e. $-\mathcal{L}_h\phi \geq 1$, a fact we will use later. The DMP is as stated here:

$$-\mathcal{L}_h V_P \leq 0 \quad \text{in } G \Rightarrow \max_{P \in G} V_P \leq \max_{P \in \partial G} \{V_P, 0\}$$

To show L^∞ -stability, we need to show that $\|\vec{e}\|_\infty \leq D\|\vec{\tau}\|_\infty$, where \vec{e} is the vector containing all the e_P 's(the errors), and $\vec{\tau}$ contains all the local truncation errors τ_P , for some D independent of h . First we need to find the truncation error. We will do this by inserting the exact solution $u(x, y)$ into our numerical scheme, which will yield as local truncation error τ_P

$$-\mathcal{L}_h u_P = f_P + \tau_P \quad (5)$$

Taylor expanding each u -term in (3) gives us the following expression for the truncation error when we solve (5) with respect to τ_P :

$$\tau_P = -\frac{1}{12}h^2((a+1)u_{xxxx} + 4u_{xxxy} + 6u_{xxyy} + 4u_{xyyy} + u_{yyyy}) + O(h^3). \quad (6)$$

For the truncation error to be bounded, we need to bound our fourth derivatives, which we bound by:

$$K = \max_{P \in [0,1]^2} \{|u_{xxxx}|, |u_{xxxy}|, |u_{xxyy}|, |u_{xyyy}|, |u_{yyyy}|\}.$$

This gives us

$$|\tau_P| \leq \frac{1}{12}h^2 K(a+1+4+6+4+1) \leq \frac{a+16}{12}h^2 K,$$

and finally,

$$\tau = \|\vec{\tau}\|_\infty = \frac{a+16}{12}h^2 K.$$

We now look at $V_P = e_P - \tau\phi$, and utilise the DMP to get a well defined error bound. By inserting this V_P into our scheme, we get

$$-\mathcal{L}_h V_P = -\mathcal{L}_h e_P + \tau\mathcal{L}_h\phi = \tau_P + \tau\mathcal{L}_h\phi \leq \tau_P - \tau \leq 0. \quad (7)$$

Here we used the result that $-\mathcal{L}_h\phi_P \geq 1$, which we showed in (4). From (7) the DMP condition is fulfilled, this in addition to the result we used gives us that the scheme is L^∞ -stable. We have from the DMP that:

$$\begin{aligned} \max_{P \in G} V_P &\leq \max_{P \in \partial G} \{V_P, 0\} \\ \max_{P \in G} \{e_P - \tau\phi\} &\leq \max_{P \in \partial G} \{e_P - \tau\phi, 0\} = 0 \\ \implies e_P - \tau\phi &\leq 0 \\ e_P &\leq \tau\phi \leq \frac{1}{8}\tau \end{aligned}$$

If we repeat the same argument with $V_P = -e_P - \tau\phi$, we will see that

$$-e_P - \tau\phi \leq 0 \Rightarrow -e_P \leq \tau\phi \leq \frac{1}{8}\tau,$$

which shows us that the scheme is L^∞ -stable. Furthermore, we get the following expression for the error bound:

$$|e_P| \leq \frac{1}{8}\tau \leq \frac{1}{8} \frac{a+16}{12}h^2 K. \quad (8)$$

Then

$$\|e\|_\infty \leq \frac{a+16}{96}h^2 K = \frac{a+16}{96}h^2 K.$$

As $\|\vec{e}\|_\infty \propto h^2$, we can conclude that the rate of convergence for smooth functions is 2 for this scheme.

2.2 Application and accuracy on the unit grid

To solve the PDE for anisotropic heatflow on the unit grid $[0, 1] \times [0, 1]$ using a numerical scheme, a rather large system of equations must be solved. Using dirichlet boundary conditions we need to solve for all the internal points of the grid at once, as most of them depend on each other, and the neighboring boundaries. Practically this means that, if we have M rows, and N columns, we must solve the system

$$A\mathbf{U} = \mathbf{F} \quad (9)$$

where A is an $(M \cdot N) \times (M \cdot N)$ dimensional matrix, \mathbf{U} is a vector containing all the grid points, and \mathbf{F} holds values for internal heat sources as well as the boundary values.

Flattening the discretized by concatenating the rows in order, we get the shape of \mathbf{U} , and likewise \mathbf{F} . The system matrix A then constructed by using the numerical scheme on all the internal points, getting an equation for each of them. In the end the matrix will have a "banded like" structure, with non-zero elements appearing only on the diagonal, and 4 off-center diagonals. This means algorithms specialized in solving sparse systems are preferable as we begin refining the grid.

To get started with a "simple" case, we set $r = 1$ and look at a couple boundaries and heat sources. By setting $r = 1$ we can use the same step size in the x- and y-directions, and thus solve $A\mathbf{U} = \mathbf{F}h^2$. Further, we set $a = 2$, as to get equal heat flow along \vec{d}_1 and \vec{d}_2 . To show the system structure, here as visualization of the matrix A , given an 8x8 grid:

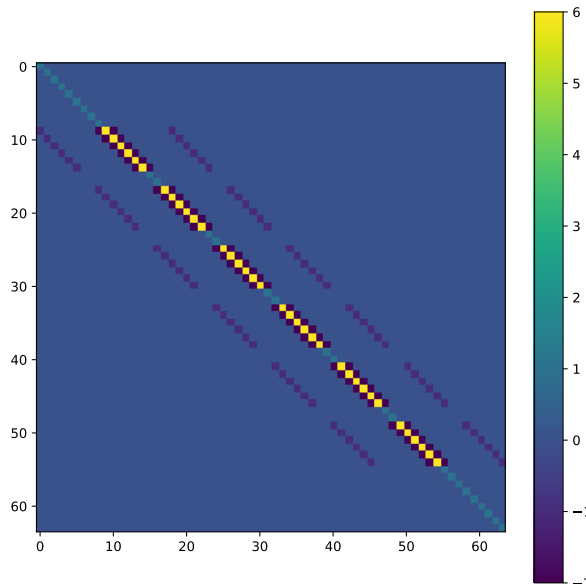


Figure 2: The system matrix A , given $M=N=8$, $a = 2$ and $r=1$.

Note the diagonal elements in light green, which are valued as 1. These are the boundary values, which we already know, and thus do not depend on elements from other rows.

At last we can solve the PDE, here are two solutions on 80x80 grids, one with a single constant boundary, and another with an internal heat source and zero-boundaries:

Satisfied that we are able to solve the PDE, we now wish to study how good our solver is. To do this we must modify the vector \mathbf{F} such that we can force a known solution, and see how close we get. This is done by finding the analytical equivalent of our numerical scheme; $\mathcal{L}\mathbf{U}$, and using it as the internal heat source. Meanwhile the boundary values are set to be equivalent to the solution we are forcing. To test error and convergence we use a polynomial:

$$f(x, y) = x^3 + 2y^2 \quad (10)$$

Using the difference operator we get our heat source as:

$$\mathcal{L}f = -(a + 1)6x - 4 \quad (11)$$

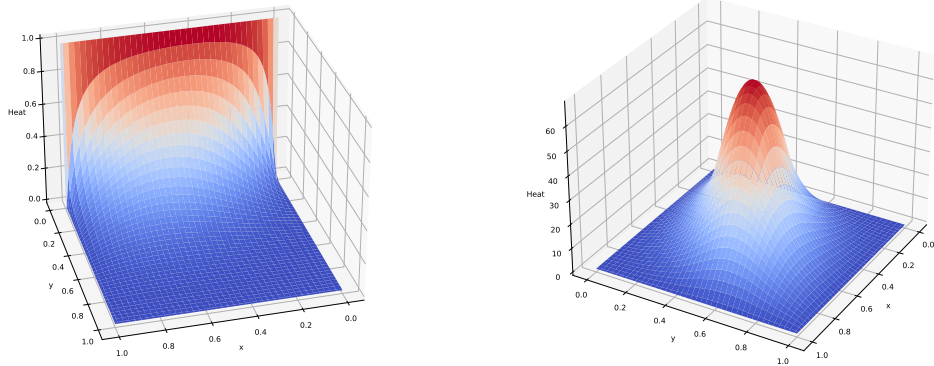


Figure 3: Left: solution with $(x,0) = 1$. Right: Solution with $F([0.375, 0.625]^2) = 1$

Successively refining our grid from 10×10 to 500×500 , then comparing the largest error on the second to last row in each case, and finally plotting step sizes against errors we get the following:

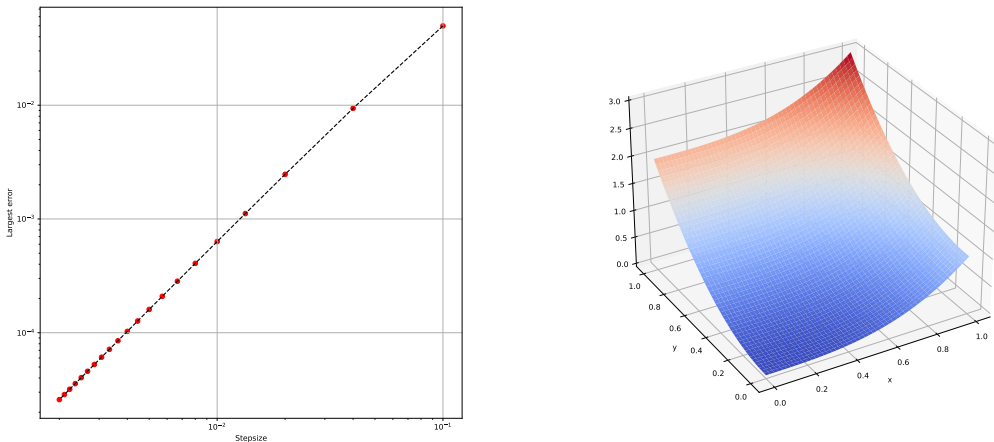


Figure 4: Left: A loglog plot of error against stepsize. Right: Numerical solution on a 500×500 grid

The first observation is that the largest error found decreases linearly with the step size in the logarithmic plot, which is good. Further, using linear regression the growth rate is found to be 1.952, which indeed means a convergence rate of approximately order 2, this is as predicted in the analysis.

Note: If we instead looked at the largest error on the entire grid, rather than the same row/column, we would get a convergence rate of order 1 instead.

2.3 A new direction

To see other limits of our model we will now look into another case of anisotropic heatflow, now with r being an irrational number. This means we must adjust our grid, so our stencil still works. To accomplish this let $h = \frac{1}{N}$ be the step size in the x-direction, and $k = |r|h$ be the step size in the y-direction. This however leads to an issue, as we have to take M steps to reach $y = 1$ we get

$$M|r|h = 1 \quad (12)$$

This implies r can be expressed as a ratio of other numbers, which is impossible, as r is irrational. In other words, we will not hit the y-boundary at $y = 1$ with a completely regular grid. One solution to this problem,

is to change the last step in the grid, and then use a central difference with two different step sizes at the end. We define k' as the last step size, and get a central difference for the last row of internal grid points:

$$\delta_y^2 U_m^n = \frac{2}{k+k'} \left(\frac{U_{m+1}^{n+1} - U_m^n}{k'} - \frac{U_m^n - U_{m-1}^{n-1}}{k} \right) \quad (13)$$

Implementing the above expression on the last row of internal points in the system matrix we can see the change:

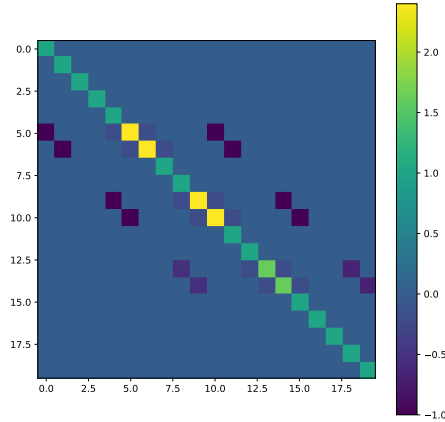


Figure 5: The system for a 5x4 grid, with $r = \sqrt{2}$

It might be hard to tell the colors apart, but in the above figure one can see that the last row of internal points depend differently to their surroundings than the earlier rows. Choosing $r = \sqrt{2}$, we can now refine the grid and solve with Dirichlet conditions:

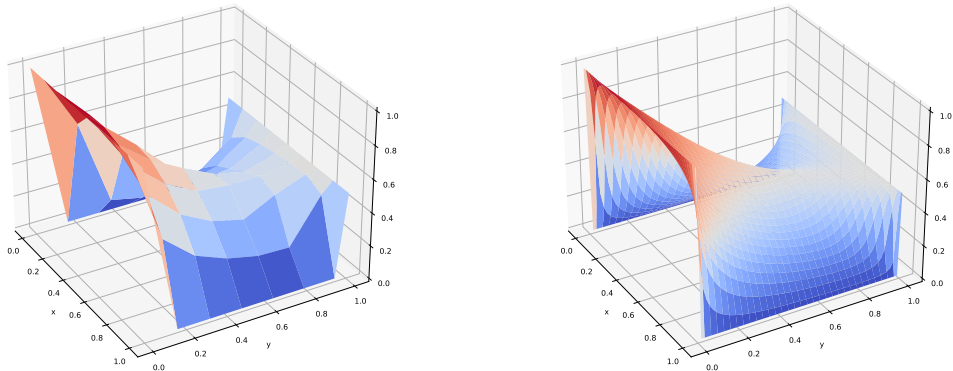


Figure 6: The same boundary value problem solved at 2 degrees of fineness.

Looking at the left figure, the short step at the end is clearly visible, and as seen on the right figure, refining the grid does not seem to cause any problems. One should note though, as $k = |r|h$ we cannot determine the number of rows on the grid freely. M is a function of k , and is found to be $M = \lfloor \frac{1}{k} \rfloor + 1$, where the "plus one" is for the shorter step, which is $k' = 1 \bmod k$.

Next we should look into how this adjustment effects the order of convergence. The error analysis is done very similarly to the previous one, with only minor adjustments to the python code. However, two different known solutions were tried, the previous polynomial, and $u(x, y) = e^{-x} \cos(y)$ for the sake testing, while the cross-derivative $\partial_x \partial_y$ is nonzero.

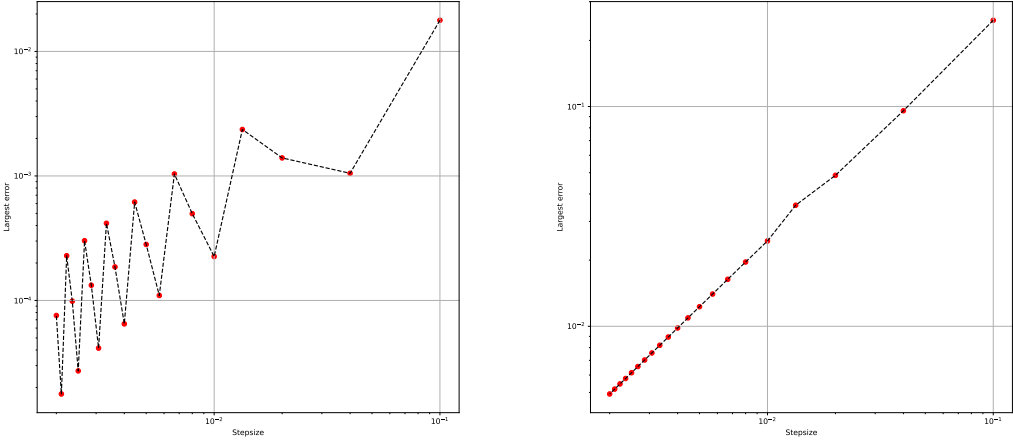


Figure 7: Logarithmic error for irrational direction $r = \sqrt{2}$. Left: $u(x, y) = e^{-x} \cos(y)$. Right: $u(x, y) = x^3 + 2y^2$.

We can safely state the convergence for the modified grid behaves differently. Given the same polynomial we used earlier we now have convergence of order 1, this is seen visually and confirmed numerically to be of order 1.0004. Meanwhile the other function behaves erratically, but does seem to improve over all as the step size decreases, linear regression gives an order of convergence at 1.296.

Finally, for the sake of plotting an extremely anisotropic case, we've set $r = \pi^2$, and then made heatflow along \vec{d}_1 about 100 times more prominent than along \vec{d}_2 :

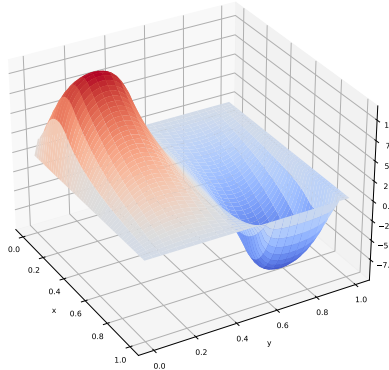


Figure 8: Highly anisotropic heatflow

2.4 Isotropic case on unit disk in first quadrant

For this next part, we will look at the isotropic case, that is, when $\kappa = I$, so we get

$$\nabla(\kappa \cdot \nabla T) = \Delta T = (\partial_x^2 + \partial_y^2)T,$$

thus making this our PDE: $-\Delta T = f$. Discretizing the PDE yields the following scheme:

$$-\mathcal{L}_h U_P = \frac{1}{h^2} (4U_P - U_N - U_E - U_S - U_W) = f_P \quad (14)$$

For simplicity, we have used equal step sizes in x- and y-direction. For the first strategy we will attempt to handle the irregular grid by modifying the scheme near the boundary, i.e for interior points where the east and/or north points end up outside our domain. We modify the stencil for these points by moving the east and

north nodes to the boundary. We denote η_1 as the distance from central node to the new east node, and η_2 as the distance from the central node to the new north node. Modifying the scheme yields the following:

$$-\tilde{\mathcal{L}}_h U_P = \frac{2}{h^2} \left(\left(\frac{1}{\eta_1} + \frac{1}{\eta_2} \right) U_P - \frac{1}{\eta_2^2 + \eta_2} U_N - \frac{1}{\eta_2 + 1} U_S - \frac{1}{\eta_1 + 1} U_W - \frac{1}{\eta_1^2 + \eta_1} U_E \right), \quad (15)$$

Where we obviously have $\eta_1 \leq 1$ and $\eta_2 \leq 1$. For the second strategy, fattening the boundary, we simply extend the boundary so that the interior points' stencils don't end up outside the domain. We extend the boundary to $\{(x, y) : 1 \leq x^2 + y^2 \leq (1+q)^2\}$.

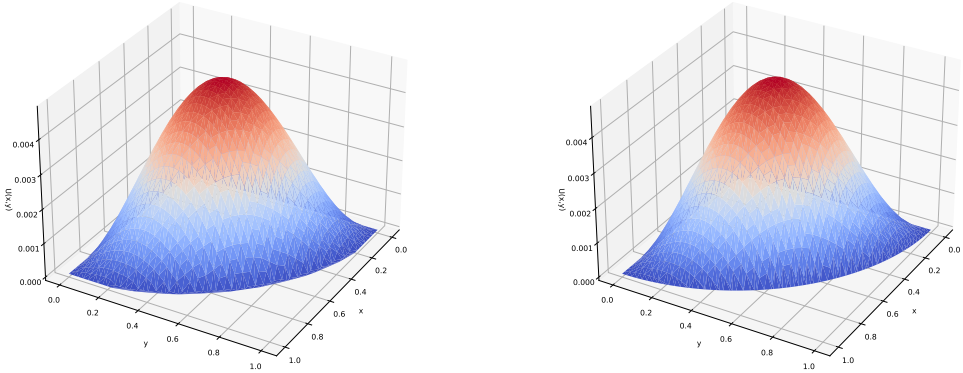


Figure 9: Left: Plot of solution using fattening of the boundary. Right: Plot of solution using modified FDM scheme.

In both cases we used $N = 40$ and $f(x, y) = xy(1 - x^2 - y^2)$. The boundary was fattened by $q = 0.03$. The strategy involving fattening the boundary was much easier to both figure out and implement, because there is no need for modifying the scheme.

3 A variable coefficient transport equation

3.1 Theory

In this case we are looking at the following equation:

$$u_t + a(x, t)u_x = 0. \quad (16)$$

Firstly we want to discretize the equation above when $a > 0$. In this case we introduce $a^+ = \max\{a, 0\}$ and use backward differences in space since we are propagation from left to right. Then the discretization becomes:

$$\frac{U_m^{n+1} - U_m^n}{k} + a^+ \frac{U_m^n - U_{m-1}^n}{h} = 0. \quad (17)$$

Further we need to look at the case when $a < 0$. In this case, we introduce $a^- = (-a)^+$ and use Forward difference in space since we are propagation from right to left. Then the discretization becomes:

$$\frac{U_m^{n+1} - U_m^n}{k} - a^- \frac{U_{m+1}^n - U_m^n}{h} = 0. \quad (18)$$

We combine (17) and (18) and end up with the following Upwind scheme:

$$\frac{U_m^{n+1} - U_m^n}{k} + a^+ \frac{U_m^n - U_{m-1}^n}{h} - a^- \frac{U_{m+1}^n - U_m^n}{h} = 0. \quad (19)$$

We collect terms in (19) and have the expression:

$$U_m^{n+1} = U_m^n \left(1 - \frac{ka^-}{h} - \frac{ka^+}{h} \right) + \frac{ka^+}{h} U_{m-1}^n + \frac{ka^-}{h} U_{m+1}^n$$

Let $r^+ = \frac{ka^+}{h}$ and $r^- = \frac{ka^-}{h}$. This gives:

$$U_m^{n+1} = U_m^n(1 - r^- - r^+) + r^+U_{m-1}^n + r^-U_{m+1}^n.$$

Studying the coefficients in front of the U-terms we find that the coefficient α in front of U_m^{n+1} , equals 1. Further the sum β of the coefficients in front of the U-terms on the right hand side are positive, thus we find $\beta = 1 - r^- - r^+ + r^+ + r^- = 1$. This leads to the condition $\alpha \geq \beta$ being fulfilled. We then use the CFL condition $1 - r^+ - r^- = 1 - |r| > 0 \Rightarrow 1 > |r|$, and have thus shown that the scheme is monotone.

Further we want to show that the upwind scheme is von Neumann stable under a CFL condition. To accomplish this we begin by looking at solutions of the form $U_m^n = \xi^n e^{i\beta x_m}$. When inserting this solution into the upwind scheme, we get:

$$\xi^{n+1} e^{i\beta x_m} = \xi^n e^{i\beta x_m} (1 - r^- - r^+) + r^+ \xi^n e^{i\beta x_{m-1}} + r^- \xi^n e^{i\beta x_{m+1}} \quad (20)$$

We solve the equation above with respect to ξ , and end up with the following expression:

$$\xi = 1 - |r| + r^+ e^{-i\beta h} + r^- e^{i\beta h}, \quad (21)$$

where we have used that $|r| = r^+ + r^-$. Next we take the absolute value of both sides of (21), and get:

$$|\xi| \leq 1 + |r| + |r^+| + |r^-| \leq 1 + 2|r| \leq 1 + \frac{2|a|}{h}k = 1 + \mu k.$$

Thus we have shown that the upwind scheme is von Neuman stable under a CFL condition. Now we want to check if the scheme is dissipative and dispersive. We use the upwind scheme, but now use the solution on the form:

$$U_m^n = \rho^n e^{i(\omega t_n + \beta x_m)} \quad (22)$$

Insert this in the upwind scheme, and get

$$\rho^{n+1} e^{i(\omega(t_n+k) + \beta x_m)} = \rho^n e^{i(\omega t_n + \beta x_m)} (1 - r^- - r^+) + r^+ \rho^n e^{i(\omega t_n + \beta(x_n-h))} + r^- \rho^n e^{i(\omega t_n + \beta(x_m+h))},$$

which reduces to the following expression:

$$\rho e^{i\omega k} = (1 - r^- - r^+) + r^+ e^{-i\beta h} + r^- e^{i\beta h}. \quad (23)$$

We know that the scheme is dissipative if $\rho < 1$. Using the fact that $e^{i\theta} = \cos \theta + i \sin \theta$, we get the following:

$$\begin{aligned} \rho e^{i\omega k} &= (1 - |r|) + r^+ (\cos \beta h - i \sin \beta h) + r^- (\cos \beta h + i \sin \beta h) \\ &= \text{Re} + i\text{Im} \\ &= 1 - |r| + (r^+ + r^-) \cos \beta h + i(r^- - r^+) \sin \beta h \\ \implies \rho^2 &= \text{Re}^2 + \text{Im}^2 = (1 - |r| + |r| \cos \beta h)^2 + r^2 \sin^2 \beta h \\ &\dots \\ &= 1 - (4|r| - 4r^2) \sin^2 \frac{\beta h}{2} < 1 \quad \text{when } |r| < 1. \end{aligned}$$

Thus we have shown that the upwind scheme is dissipative when $|r| < 1$. Further we evaluate whether the scheme is dispersive. For this we need to show whether $\omega k = \arg(\text{Re} + i\text{Im}) = \arctan(\frac{\text{Im}}{\text{Re}})$ is not linear in βh . We insert our values for Re and Im and get the following expression:

$$\omega k = \arctan \left(\frac{-r \sin \beta h}{1 - |r| + |r| \cos(\beta h)} \right). \quad (24)$$

We can from this see that ωk is not linear in $\beta h \Rightarrow$ the scheme is dispersive.

The Lax-Wendroff scheme is derived by using the Taylor series expansion to achieve second accuracy in space and time. We start by rewriting the equation $U_t + aU_x = 0$:

$$u_t = -au_x \Rightarrow u_{tt} = -a(x)u_{tx} = -a(x)(u_t)_x = -a(x)(-a(x)u_x)_x = a(au_x)_x.$$

We use Taylor in time and get:

$$u_m^{n+1} = u + ku_t + \frac{1}{2}k^2u_{tt} + O(k^3) = u - kau_x + \frac{1}{2}k^2a(au_x)_x + O(k^3)$$

Use Forward Euler on u_x and u_{xx} and the Taylor expansion in time, then we get the Lax- Wendroff scheme as:

$$U_m^{n+1} = U_m^n - ka \frac{U_{m+1}^n - U_{m-1}^n}{2h} + \frac{1}{2}k^2aa_x \frac{U_{m+1}^n - U_{m-1}^n}{2h} + \frac{1}{2}(ka)^2 \frac{U_{m+1}^n - 2U_m^n + U_{m-1}^n}{h^2} \quad (25)$$

We let $r = \frac{ka}{h}$ and collect terms, then we can rewrite the scheme as:

$$U_m^{n+1} = U_m^n(1 - r^2) + U_{m+1}^n \left(\frac{kra_x}{4} - \frac{r}{2} + \frac{r^2}{2} \right) + U_{m-1}^n \left(\frac{r^2}{2} - \frac{kra_x}{4} + \frac{r}{2} \right). \quad (26)$$

3.2 Results

To see how good the Upwind- and Lax-Wendroff-schemes are, we again have to study their convergence as we decrease the step sizes. As both methods depend on both step size in space, h , and time, k , we need spacial and temporal convergence rates for each method. Comparing the numerical solutions to analytic ones leads to incorrect rates for these methods, so both them will be compared to the numerical solution at $M = 1000$, and $N = 10000$. First, Lax-Wendroff:

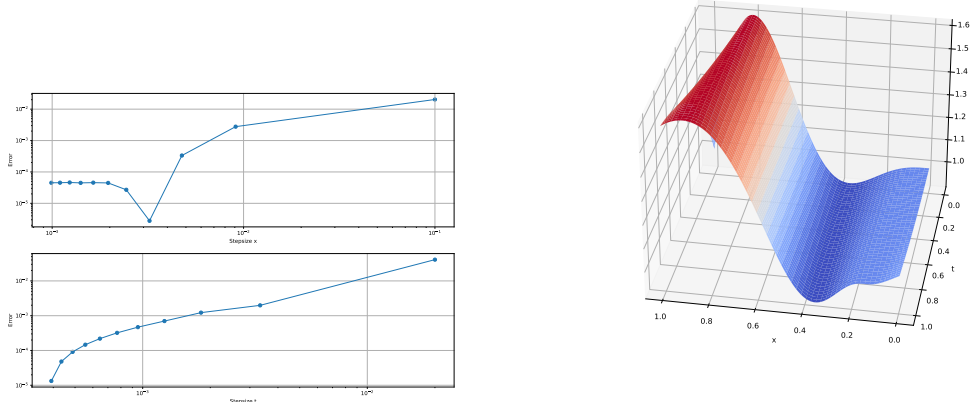


Figure 10: Left: Lax-Wendroff spacial and temporal convergence rates. Right: 1000×2500 solution

For the Law-Wendroff scheme the spacial and temporal convergence rates were found by linear regression to be approximately 1.51 and 1.71, respectively. These rates could fluctuate somewhat with the grid fineness, but these rates were most common. Next is the Upwind scheme:

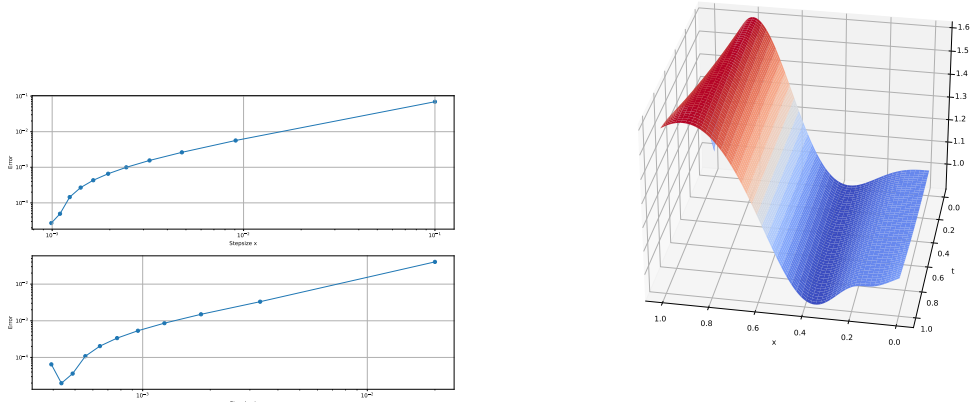


Figure 11: Left: Spacial and temporal Upwind convergence rates. Right: 1000×2500 solution.

These results are very comparable to the Lax-Wendroff scheme, the convergence rates were approximately 1.55 and 1.82 with respect to space and time, respectively. Again, these rates could fluctuate somewhat, with choice of grid, and where we chose to measure the error.

4 Conclusion

Summing up this report, we have looked at how to solve elliptic partial differential equations on differing grids. We've looked into how irregular grids change convergence, error and ease of scheme implementation. Further we also looked into a hyperbolic PDE, and studied two solution schemes, and their convergence.

The work was roughly evenly distributed among the group members.